Vortex-line fluctuations in model high-temperature superconductors

Ying-Hong Li
Institute for Theoretical Physics, University of Utrecht, 3508 TA Utrecht, The Netherlands

S. Teitel
Department of Physics and Astronomy, University of Rochester, Rochester, New York 14627
(Received 15 June 1992)

We carry out Monte Carlo simulations of the uniformly frustrated three-dimensional XY model, as a model for vortex-line fluctuations in a high-T_c superconductor in an external magnetic field. A density of vortex lines of $f = \frac{1}{25}$ is considered. We find two sharp phase transitions. The low-T superconducting phase is an ordered vortex-line lattice. The high-T normal phase is a vortex-line liquid, with much entangling, cutting, and loop excitations. An intermediate phase is found, which is characterized as a vortex-line liquid of disentangled, approximately straight, lines. In this phase, the system displays superconducting properties in the direction parallel to the magnetic field, but normal behavior in planes perpendicular to the field. A detailed analysis of the vortex structure function is carried out.

I. INTRODUCTION

While an understanding of the microscopic mechanism leading to high-temperature superconductivity has remained elusive, much recent research has focused on obtaining a phenomenological understanding of the behavior of these materials in the presence of applied currents and magnetic fields. Such treatments have been based on the familiar Landau-Ginzburg approach for type-II superconductors, which assumes only that macroscopically, the superconductivity is adequately described by a complex order parameter, as is the case for classical BCS materials. In this context, the high-T_c materials are generally believed to differ from the classical superconductors in that fluctuation effects are dramatically enhanced.[1–3] The relatively high values of T_c, anisotropy, and ratio of magnetic penetration to coherence lengths, $\kappa = \lambda/\xi_0$, in these materials lead to a significantly larger critical region in temperature, about T_c.

In the presence of an applied magnetic field $H_{c1} < H < H_{c2}$, the low-temperature phase of a pure system is the Abrikosov vortex-line lattice. As temperature increases, it has been argued that fluctuations will cause this vortex-line lattice to melt at a temperature well below that given by the mean field $H_{c2}(T)$ line, leading to a vortex-line liquid phase.[1–5] Experimental evidence for such a scenario has been cited in mechanical oscillator measurements,[6] as well as by the observation that the onset of sizable reversible magnetization generally occurs at a temperature well above that where resistivity vanishes,[7] an indication of strong fluctuation effects. Several theoretical works have sought to describe the nature of this vortex-line lattice melting transition, as well as predict properties of the vortex-line liquid phase. One commonly used approach is an effective elastic theory,[1,3–5] in which the energy of transverse fluctuations of the vortex lines from their lattice positions is computed in terms of nonlocal elastic constants determined from the mean field Landau-Ginzburg theory.[8] The Lindemann criterion is then used to estimate melting when such transverse fluctuations become a sizable fraction of the vortex-line spacing. Another theoretical model has been the "two-dimensional boson" approximation[1,2,9] in which vortex lines, fluctuating in a directed fashion along the direction of the applied magnetic field, are viewed as the "world lines" of two-dimensional (2D) interacting bosons. Many-body methods applied to the two-dimensional boson problem have then been used to estimate melting in the dilute line limit,[1,2] as well as to compute properties of the vortex-line liquid.[1,9]

The above theoretical models suffer from several important limitations. The effective elastic theory loses validity once the vortex lines are in a liquid phase. The "2D boson" approximation assumes a simplified vortex-line interaction, that applies mainly when lines do not wander too much from parallel alignment with the applied magnetic field. Both models assume that the vortex lines thread the system in a directed fashion; each line passes through each plane perpendicular to $\mathbf{B}$ only once. Closed vortex-line loop excitations, which have been argued to play a significant role in the $\mathbf{B} = \mathbf{0}$ case[3,10] as well as in the finite $\mathbf{B}$ case[11] are ignored. In view of this, it is useful to have a well-defined statistical model, for which numerical simulations can be carried out, and in which the effects of vortex-line fluctuations may be quantitatively examined.

In this paper we present the results of such a study, based on a simplified model which we believe captures the essential physics of a fluctuating Landau-Ginzburg superconductor; the uniformly frustrated three-dimensional

XY model. We have previously introduced this model in two earlier works.[12,13] Here we provide details, as well as surprising results. We find that as the vortex-line lattice is heated, the system undergoes two distinct thermodynamic transitions. First there is a transition characterized by the loss of phase coherence in planes perpendicular to the applied magnetic field, while phase coherence is retained parallel to the field. In this intermediate region, the vortex-line lattice disorders in the transverse direction, while individual lines remain essentially straight and unentangled from each other. Then at a higher temperature, phase coherence is lost in the direction parallel to $\mathbf{B}$ as well. This high-temperature region is characterized by vortex-line wandering and many closed loop excitations. The vortex lines are highly entangled, yet they easily cut through one another.

The remainder of our paper is organized as follows. In Sec. II we present a detailed description of our model, and the approximations involved. In Sec. III we present the results of our Monte Carlo simulations: Sec. III A discusses computation of the helicity moduli, which measure the loss of phase coherence; Sec. III B discusses the nature of vortex-line fluctuations in the various thermodynamic phases; and Sec. III C presents a detailed analysis of the vortex structure function, which is used to extract effective elastic constants and correlation lengths. In Sec. IV we summarize our conclusions.

II. DESCRIPTION OF THE MODEL

It is generally believed that the phenomenological behavior of the high-temperature superconductors is well described by the familiar Landau-Ginzburg free energy functional,[14]

$$F[\psi(\mathbf{r}),\mathbf{A}(\mathbf{r})]=\int d^3r\left\{\alpha|\psi|^2+\frac{1}{2}\beta|\psi|^4+\frac{\hbar^2}{2m}\left|\left(-i\boldsymbol{\nabla}+\frac{2\pi}{\Phi_0}\mathbf{A}\right)\psi\right|^2+\frac{1}{8\pi}|\boldsymbol{\nabla}\times\mathbf{A}|^2\right\}, \tag{1}$$

where ψ is the superconducting order parameter, $\mathbf{A}$ the magnetic vector potential, and $\Phi_0=hc/2e$ the flux quantum. The local magnetic induction is $\mathbf{b}(\mathbf{r})=\boldsymbol{\nabla}\times\mathbf{A}(\mathbf{r})$. The first two terms represent the condensation energy, the third term is the kinetic energy of the flowing supercurrents, and the fourth term is the magnetic field energy. We choose to work throughout this paper with the *Helmholtz* free energy, which is a function of the average magnetic induction, $\mathbf{B}=(1/\mathrm{Vol})\int d^3r\,\mathbf{b}(\mathbf{r})$, inside the bulk superconductor. The applied magnetic field $\mathbf{H}$ may in principle be determined by an appropriate thermodynamic derivative of the Helmholtz free energy, but its value is of no direct concern for our calculations. For simplicity, we consider here only a material with isotropic couplings, and indicate later how the effects of anisotropy may be included in our model.

The mean field solution, appropriate for low-temperature superconductors, is obtained by minimizing Eq. (1) with respect to both ψ and $\mathbf{A}$, subject to the constraint of constant $\mathbf{B}$. For $\mathbf{B}=\mathbf{0}$, one gets the uniform solution $\psi(\mathbf{r})=\sqrt{|\alpha|/\beta}\equiv\psi_0$ in the superconducting phase, $\alpha<0$ ($\psi_0=0$ in the normal phase, $\alpha>0$). For $0<B<H$, in the mixed phase of a type-II superconductor, the result is the familiar Abrikosov flux tube lattice.[14] Each flux tube carries one Φ_0 of flux, and consists of a vortex line in the phase $\theta(\mathbf{r})$ of $\psi(\mathbf{r})=|\psi(\mathbf{r})|e^{i\theta(\mathbf{r})}$. The vortex line is surrounded by a normal region of radius the coherence length,

$$\xi_0=\hbar/\sqrt{2m|\alpha|} \tag{2}$$

and the magnetic field is confined to within a region of radius the magnetic penetration length,

$$\lambda=\sqrt{mc^2/16\pi e^2|\psi_0|^2}. \tag{3}$$

The density of flux tubes is B/Φ_0, hence the separation between vortex lines is

$$a_v\simeq\sqrt{\Phi_0/B}. \tag{4}$$

For the high-temperature superconductors, we now wish to compute thermodynamic quantities, averaging over all fluctuations of ψ and $\mathbf{A}$ (subject to the constraint of constant $\mathbf{B}$), weighting configurations with the Boltzman factor $e^{-F[\psi,\mathbf{A}]/k_BT}$. In order to carry out this average numerically, with Monte Carlo simulations, we make the following approximations.

For $\lambda\gg a_v$, the magnetic fields of the individual flux tubes strongly overlap, leading to an approximately uniform local magnetic induction. In this limit, we therefore make the approximation of replacing the fluctuating $\mathbf{A}$ with a fixed one, giving a spatially uniform magnetic induction $\mathbf{B}=\boldsymbol{\nabla}\times\mathbf{A}$. We will discuss the consequences of this approximation on the effective vortex-line interaction in more detail below. Next we discretize[15] our model by placing it on a periodic cubic mesh of lattice constant a, resulting in the free energy functional

$$F[\psi_j,A_{ij}]=a^3\sum_j\left\{\left(\alpha+\frac{\hbar^2}{2ma^2}\right)|\psi_j|^2+\frac{1}{2}\beta|\psi_j|^4\right\}-\frac{a\hbar^2}{2m}\sum_{\langle ij\rangle}\psi_j^*e^{-iA_{ij}}\psi_i+\text{c.c.}, \tag{5}$$

where we have dropped the now constant magnetic energy term. Here i,j denote sites of the cubic mesh, $\langle ij\rangle$ denote nearest-neighbor bonds of the mesh, and

$$A_{ij}\equiv\frac{2\pi}{\Phi_0}\int_i^j\mathbf{A}\cdot d\boldsymbol{l}. \tag{6}$$

Finally, we choose the lattice constant of the numerical mesh $a=\xi_0$, the coherence length of Eq. (2). Thus the decay to zero of the superconducting wave function ψ at the normal core of a vortex line takes place within one unit cell of the mesh. Outside the normal core, we can make a London approximation and set $|\psi|=\psi_0$, a constant. Thus on the mesh, we consider only fluctuations

of the form $\psi_j = \psi_0 e^{i\theta_j}$, where the amplitude is fixed, and only the phases θ_j vary. Details concerning the normal cores of vortex lines are treated approximately by the small length cutoff $a = \xi_0$ imposed by the mesh. Applying this to the free energy in Eq. (5) results, within additive constants, in the effective Hamiltonian for a frustrated three-dimensional XY model,

$$F[\theta_i] = -J_0 \sum_{\langle ij \rangle} \cos(\theta_i - \theta_j - A_{ij}), \tag{7}$$

where Eqs. (3) and (5), $\Phi_0 = hc/2e$, and $\xi_0 = a$ give

$$J_0 = \frac{\Phi_0^2 \xi_0}{16\pi^3 \lambda^2}. \tag{8}$$

Anisotropy, or impurities, could now easily be incorporated into the model by letting the coupling J_0 vary appropriately on different bonds of the mesh. In this work we continue to consider only the case of isotropic couplings. We expect that the *qualitative* behaviors we find will be to a large extent the same as in anisotropic systems.[12,16]

The Hamiltonian (7) above has been studied extensively in two dimensions as a model for Josephson junction arrays,[17,18] and in two and three dimensions as a model for granular superconductors.[19] Its application to behavior in the high-temperature superconductors is best realized in the limit $\xi_0 \ll a_v \ll \lambda$, where the above approximations should apply. This condition may be rewritten[14] as $H_{c1} \ll H \ll H_{c2}$. For the high-T_c materials, where $\kappa = \lambda/\xi_0 \sim 100$ is large, this will cover a large range of experimentally accessible magnetic fields H. For YBaCuO, for example, this condition holds for fields on the order of a few Tesla.

Much of the theoretical work concerning fluctuations in the high-T_c superconductors has been discussed in terms of fluctuations of the vortex lines induced by a finite B. It is therefore of interest to consider the effective vortex-line interaction in our model (7). Towards this end, it is convenient to replace the cosine function of Eq. (7) with the periodic Gaussian or Villain function:[20]

$$F[\theta_i] = J_0 \sum_{\langle ij \rangle} V(\theta_i - \theta_j - A_{ij}), \tag{9}$$

where

$$V(\alpha) \equiv -(T/J_0) \ln \left\{ \sum_{m=-\infty}^{\infty} \exp\left[-\frac{1}{2} J_0 (\alpha - 2\pi m)^2 / T \right] \right\}. \tag{10}$$

This has the effect of eliminating the coupling between spin wave and vortex excitations of the phase variables θ_i in the Hamiltonian (7).

Making a standard duality transformation[21] on this new Hamiltonian (9) gives the effective Hamiltonian in terms of the vortex degrees of freedom:

$$F_v[n_\mu(i)] = 2\pi^2 J_0 \sum_{i,j} \sum_{\mu} [n_\mu(i) - f_\mu(i)] \times [n_\mu(j) - f_\mu(j)] G(\mathbf{r}_i - \mathbf{r}_j). \tag{11}$$

Here $n_\mu(i)$ is the integer vorticity in the phase θ going around the plaquette with normal $\hat{\boldsymbol{\mu}} = \hat{\mathbf{x}}, \hat{\mathbf{y}}, \hat{\mathbf{z}}$ of the cubic unit cell centered at the dual mesh site i, and $f_\mu(i)$ is the number of flux quanta of magnetic induction through this plaquette,

$$2\pi f_\mu(i) = \frac{2\pi}{\Phi_0} \oint \mathbf{A} \cdot d\boldsymbol{l} = A_{jk} + A_{kl} + A_{lm} + A_{mj}, \tag{12}$$

where the sum is taken counterclockwise over the bonds forming the edges of the plaquette. For our uniform magnetic field approximation, with $\mathbf{B}$ along the $\hat{\mathbf{z}}$ direction,

$$f_z(i) = B\xi_0^2/\Phi_0 \equiv f, \quad f_x(i) = f_y(i) = 0. \tag{13}$$

In this case, the ground state of Eq. (11) will consist of a periodic structure of straight vortex lines, aligned with $\mathbf{B}$ in the $\hat{\mathbf{z}}$ direction, with density f.

The interaction potential G in Eq. (11), is the lattice Green's function which solves

$$D_{ij} G(\mathbf{r}_j - \mathbf{r}_k) = -\delta_{i,k}, \tag{14}$$

where D_{ij} is the lattice Laplacian. $G(\mathbf{r})$ is most easily expressed in terms of its Fourier transform

$$G(\mathbf{r}) = \frac{1}{N} \sum_k G_k e^{i\mathbf{k}\cdot\mathbf{r}}, \tag{15}$$

where N is the number of sites in the mesh, and

$$G_k = 1/K^2 = 1/(K_z^2 + K_\perp^2), \tag{16}$$

$$K_z^2 \equiv 2 - 2\cos k_z a, \quad K_\perp^2 \equiv 4 - 2\cos k_x a - 2\cos k_y a.$$

Note $K^2 \simeq (ka)^2$ for small ka, however they are different at large ka due to the discreteness of the mesh. For large $r \gg a$, $G(\mathbf{r}) \simeq 1/(4\pi r)$.

We thus see that the interaction between vortex lines in our model is the Coulomb interaction, $G_k = 1/K^2$. For comparison, the mean field London interaction in the continuum,[22] obtained by minimizing the free energy Eq. (1) with respect to a spatially varying $\mathbf{b}(\mathbf{r})$, is $G_k^{\text{London}} = 1/(k^2 + \lambda^{-2})$, which is a screened Coulomb interaction with screening length λ. Thus our approximation of taking a uniform magnetic induction $\mathbf{b}(\mathbf{r}) = \mathbf{B}$, and ignoring spatial variations and fluctuations in $\mathbf{b}$, corresponds formally to making this screening length infinite. Our model therefore strongly suppresses long length scale (small k) vortex-line density fluctuations, as compared to the true superconductor. However we expect that the energetics of fluctuations on small length scales $k^{-1} \lesssim \lambda$ are well approximated. Provided $a_v \ll \lambda$, the model should therefore correctly describe the high $k \sim 1/a_v$ fluctuations describing collisions between near-neighbor vortex-lines, which are believed responsible for the melting of the vortex line lattice.[4]

It will be convenient for later to write Eq. (11) in terms of Fourier transforms. Defining

$$n_\mu(\mathbf{k}) \equiv \sum_i n_\mu(i) e^{-i\mathbf{k}\cdot\mathbf{r}_i}, \tag{17}$$

we have as the Hamiltonian

$$F_v[n_\mu(i)] = \frac{2\pi^2 J_0}{N} \sum_{\mu,k\neq 0} n_\mu(\mathbf{k}) n_\mu(-\mathbf{k}) G_k. \tag{18}$$

The $k = 0$ contribution to F_v would be $[n_\mu(\mathbf{k} = 0) - Nf_\mu]^2 G_{k=0}$, where f_μ is as in Eq. (13). However as $G_{k=0}$ diverges [see Eq. (16)], the requirement that the total free energy be finite ensures that we only have configurations where the average vortex density in direction $\hat{\boldsymbol{\mu}}$ is f_μ; hence the $k = 0$ piece vanishes.

III. MONTE CARLO SIMULATIONS

To investigate the behavior of the model, we carry out Metropolis Monte Carlo simulations, of the Hamiltonian (9), on a cubic mesh with $N = L_z L_\perp^2$ sites and periodic boundary conditions in all directions. Our simulations are carried out directly in terms of the phase variables θ_i, with no additional presumptions concerning the behavior of vortex lines, beyond those implicit in Eq. (9). Simulations of this same model, only working directly in terms of the vortex variables and using the Hamiltonian (11), have recently been reported by Cavalcanti *et al.*[23]

Previously we have reported[12,13] on our simulations using a density of field induced vortex lines of $f = \frac{1}{5}$. In this work we report on simulations using a density of lines $f = \frac{1}{25}$, with an average spacing between lines of $a_v = 5a$. This value of f was chosen so as to increase the ratio a_v/a, and hence reduce effects due to the discreteness of our numerical mesh, while making f large enough so as to have a large number of lines contained within a system of computational size. Our present simulations are carried out for a mesh of size $L_\perp = 50$ and $L_z = 24$, giving 100 vortex lines in the ground state. The ground state of our system we believe to be the periodic extension of the unit cell of straight vortex lines, shown in Fig. 1. Although we have no way to prove that this is the true ground state, anealing with Monte Carlo simulations failed to result in any state with lower energy. That our presumed ground state is a square lattice of lines, instead of the triangular lattice expected in a continuum model, is due to the competition between vortex-line interactions and the cubic discreteness of our numerical mesh. Most of our calculations represent runs of 2000 Monte Carlo sweeps to equilibrate, with 20 000 sweeps for computing averages. Each Monte Carlo sweep refers to one pass through the entire cubic mesh. Errors are estimated either by block averaging, or from comparing independent runs. Henceforth we measure length in units where $\xi_0 = a = 1$, and temperature in units where $k_B = 1$.

A. Helicity modulus

The most convenient method to detect phase coherence, i.e., superconductivity in the model Hamiltonian (9), is to compute the helicity modulus.[24] The helicity modulus Υ_μ in the direction $\hat{\boldsymbol{\mu}}$ is defined as follows.[25] Imagine applying boundary conditions such that the phase across the system in the direction $\hat{\boldsymbol{\mu}}$ is twisted by an amount $L_\mu \delta$. If $\hat{\boldsymbol{\mu}} = \hat{\mathbf{x}}$, for example, we would require

$$\theta(x = L_x, y, z) - \theta(x = 0, y, z) = L_x \delta. \tag{19}$$

Now transform to the new set of variables

$$\theta_i' = \theta_i - (\mathbf{r}_i \cdot \hat{\boldsymbol{\mu}})\delta. \tag{20}$$

If θ_i obey the twisted boundary conditions (19), then these new variables θ_i' are easily seen to obey periodic boundary conditions. In terms of θ_i', the system with the twisted boundary conditions is described by the Hamiltonian

$$F[\theta_i'; \delta] = J_0 \sum_{\langle ij \rangle} V[\theta_i' - \theta_j' - A_{ij} - (\hat{\mathbf{e}}_{ij} \cdot \hat{\boldsymbol{\mu}})\delta], \tag{21}$$

where $\hat{\mathbf{e}}_{ij}$ is the unit vector from site i to site j. One can now form the partition function

$$Z(\delta) = \sum_{\{\theta_i'\}} e^{-F[\theta_i'; \delta]/T}, \tag{22}$$

where the sum is only over configurations $\{\theta_i'\}$ satisfying periodic boundary conditions. The total free energy is then

$$\mathcal{F}(\delta) = -T \ln Z(\delta) \tag{23}$$

and the helicity modulus is now defined as

$$\Upsilon_\mu \equiv \frac{1}{N} \frac{\partial^2 \mathcal{F}}{\partial \delta^2}\bigg|_{\delta=0}, \tag{24}$$

where $N = L_z L_\perp^2$. Υ_μ measures the stiffness to twisting the phase up in the $\hat{\boldsymbol{\mu}}$ direction, and may be thought of

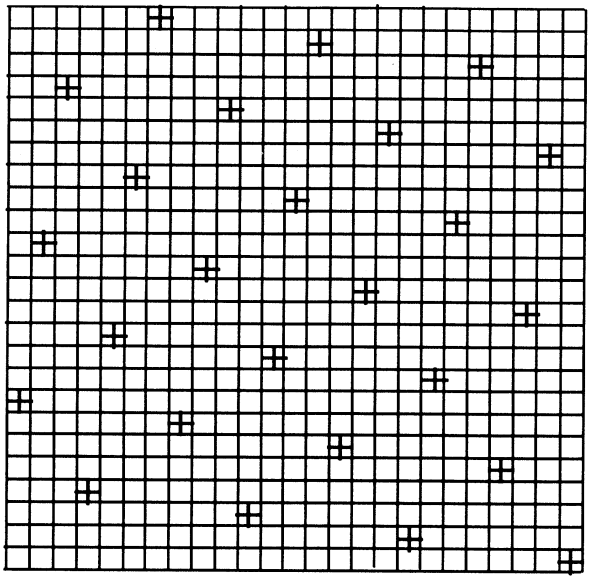

FIG. 1. Ground state vortex-line lattice for a magnetic induction of $f = B\xi_0^2/\Phi_0 = \frac{1}{25}$ flux quantum per unit cell of the numerical mesh. The view is along the direction of **B**, and (+) locates the positions of the straight vortex lines.

as the renormalized coupling J_0 on infinitely long length scales. Equivalently, Υ may be viewed as the effective superfluid density, or via Eq. (8), as determining the renormalized magnetic penetration length, $\Upsilon \sim 1/\lambda_R^2$. When $\Upsilon_\mu > 0$ there is phase coherence in the $\hat{\boldsymbol{\mu}}$ direction, and when $\Upsilon_\mu = 0$, phase coherence is lost. The vanishing of Υ_μ in a particular direction therefore signals a superconducting to normal transition.

In terms of the definitions Eqs. (21)–(24), we can write the helicity modulus as the correlation function

$$\Upsilon_\mu = \frac{J_0}{N}\left\langle \sum_{\langle ij\rangle} V''(\theta_i - \theta_j - A_{ij})(\hat{\mathbf{e}}_{ij}\cdot\hat{\boldsymbol{\mu}})^2 \right\rangle - \frac{J_0^2}{TN}\left\{ \left\langle \left[\sum_{\langle ij\rangle} V'(\theta_i - \theta_j - A_{ij})(\hat{\mathbf{e}}_{ij}\cdot\hat{\boldsymbol{\mu}}) \right]^2 \right\rangle - \left\langle \sum_{\langle ij\rangle} V'(\theta_i - \theta_j - A_{ij})(\hat{\mathbf{e}}_{ij}\cdot\hat{\boldsymbol{\mu}}) \right\rangle^2 \right\}, \tag{25}$$

which can be evaluated directly in the Monte Carlo simulation. V' and V'' are the first and second derivatives of the Villain function defined in Eq. (10).

In Fig. 2 we show our results for Υ_z and $\Upsilon_\perp \equiv \frac{1}{2}(\Upsilon_x + \Upsilon_y)$, as a function of temperature. Both heating from the ground state (Fig. 1) and cooling from random are shown. The results clearly indicate two sharp transitions. As T is increased, there is first a transition $T_{c\perp} \simeq 1.3J_0$ at which $\Upsilon_\perp \to 0$ but $\Upsilon_z > 0$. Phase coherence is lost in the directions perpendicular to the applied magnetic field, however phase coherence persists in the direction parallel to the magnetic field. Then, at a higher $T_{cz} \simeq 2.5J_0$, $\Upsilon_z \to 0$ and phase coherence is lost in the parallel direction as well, and we have the completely normal phase. In the intermediate phase, $T_{c\perp} < T < T_{cz}$,

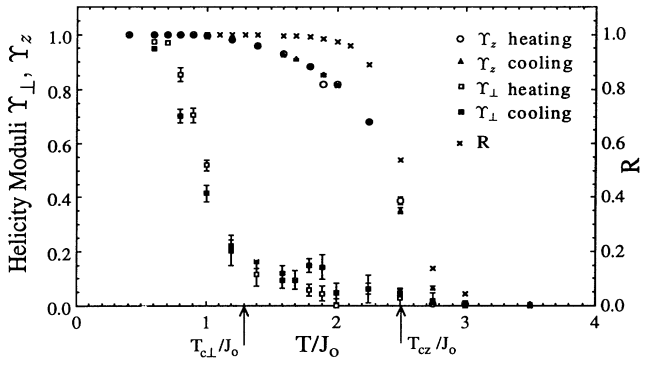

FIG. 2. Helicity modulus Υ_z along direction of **B**, and $\Upsilon_\perp$ perpendicular to **B**, for both heating and cooling. The vanishing of $\Upsilon_{z,\perp}$ indicates two separate phase transitions. R is the fraction of vortex lines which reconnect to themselves when the system is periodically extended along the $\hat{\mathbf{z}}$ direction (see Sec. III B 1). The vanishing of R indicates entanglement of lines.

the linear resistivity ρ_z parallel to **B** should vanish, however the linear resistivity $\rho_\perp$ perpendicular to **B** should remain finite. Such an intermediate phase is in complete agreement with recent predictions by Feigel'man and coworkers,[26] who used arguments based on the "2D boson" approximation. At the lower transition, $T_{c\perp}$, a slight hysteresis is seen, comparing heating versus cooling. No hysteresis is seen at T_{cz}.

B. Vortex-line fluctuations

We now seek to describe the nature of vortex-line fluctuations in the three distinct phases discussed above. We will find that the high-temperature phase is one in which vortex lines wander, entangle, and cut through each other easily. In this phase, we also find that the density of vortex lines is greatly increased by the excitation of many closed vortex loops. The intermediate phase is one in which vortex lines are unentangled, remaining on average straight and aligned with **B**, however they are in a liquid state as far as their correlations in planes perpendicular to **B** are concerned.

As our simulations are carried out in terms of the variables θ_i, we first must locate the positions of the vortex lines as they thread their way through the system. We use the following algorithm. For each plaquette α in the system, we compute

$$2\pi f_\alpha + \sum_\alpha [\theta_i - \theta_j - A_{ij}] \equiv 2\pi n_\alpha, \tag{26}$$

where the sum is taken counterclockwise around the bounds of the plaquette, f_α is the magnetic flux through the plaquette as given by Eqs. (12) and (13), and $[\theta_i - \theta_j - A_{ij}]$ are measured restricted to the interval $[-\pi, \pi]$. n_α is then the integer vorticity in θ_i going around this plaquette. As vorticity is conserved, each unit cell of the cubic mesh which has one plaquette with a vortex entering the cell has another plaquette with a vortex leaving. By computing the vorticity entering and leaving the unit cells of the mesh, we are able to trace out the paths of the vortex lines. In the event that two vortex lines enter and leave the same unit cell, we randomly assign which exiting segment is connected to which entering segment, for the purpose of identifying the paths of those lines.

1. Upper transition T_{cz}

One property that has received much theoretical attention has been the entanglement of vortex lines, once the ground state vortex-line lattice has melted. Interesting dynamical effects have been suggested assuming a large energy barrier exists against vortex lines cutting through each other.[1,2,27,28] In such a case, entanglement would provide a topological constraint limiting vortex-line motion. A single pinned line would pin the many lines with which it is entangled, substantially reducing the flux flow resistance.

In our model, it is simple to check for entanglement. We follow a prescription proposed by Nelson.[1,2] Let $\{\mathbf{r}_{\perp i}(0), \mathbf{r}_{\perp j}(0), ...\}$ be the positions of the vortex lines in the xy plane, as they pierce the plane at $z = 0$. Let $\{\mathbf{r}_{\perp i}(L_z), \mathbf{r}_{\perp j}(L_z), ...\}$ be the corresponding locations of these vortex lines as they pierce the $z = L_z$ plane. Since our simulation uses periodic boundary conditions in the z direction, parallel to $\mathbf{B}$, all the $\mathbf{r}_{\perp i}(L_z)$ must connect onto some $\mathbf{r}_{\perp j}(0)$, so that the vortex lines remain continuous in the periodically extended system. If $\mathbf{r}_{\perp i}(L_z)$ connects to $\mathbf{r}_{\perp i}(0)$, we say that line i reconnects to itself. If we view the periodic boundary condition along the $\hat{\mathbf{z}}$ direction as representing the circumference of a three-dimensional torus, then line i winds only once around the torus, before reconnecting to itself. In contrast, if $\mathbf{r}_{\perp i}(L_z)$ connects to $\mathbf{r}_{\perp j}(0)$, $j \neq i$, then lines i and j are part of a larger multiple connection of lines that winds more than once around the torus, before reconnecting to itself (see Fig. 3). For an entangled vortex-line state, we would expect there to be many such multiple connections, while for disentangled approximately straight lines, there should be only simple self-reconnections. In Fig. 2, we plot the fraction of lines which reconnect to themselves, R, versus temperature, which we compute while cooling the system from an initial random configuration. R drops sharply to zero at T_{cz}, from its low-temperature value of one. We thus identify this upper transition, where phase coherence in the direction parallel to $\mathbf{B}$ is lost, as a transition from straight disentangled lines, to wandering entangled lines. Further, the fact that the multiply connected entangled lines present at high temperature completely disentangle to simple self-reconnected lines below T_{cz}, suggests that the lines may easily cut through each other as they disentangle.

As an alternative criterion for vortex-line entanglement, we can consider the transverse fluctuations of the vortex lines $\langle u^2(l_z)\rangle$ as a function of length $0 \leq l_z \leq L_z$ parallel to $\mathbf{B}$,

$$\langle u^2(l_z)\rangle = \frac{1}{N_v l_z} \sum_{i=1}^{N_v} \sum_{z=0}^{l_z} \langle [\mathbf{r}_{\perp i}(z) - \mathbf{r}_{\perp i}(z_0)]^2 \rangle, \quad z_0 = l_z/2, \tag{27}$$

where $\mathbf{r}_{\perp i}(z)$ is the position of line i in the xy plane at z, $N_v = fL_\perp^2$ is the number of magnetic field induced lines, and the sum is along the lengths of these lines for a distance l_z. Vortex lines in our model may in general consist of two types: the magnetic field induced lines which thread the entire system from $z = 0$ to $z = L_z$, and thermally excited closed vortex loops. In the evaluation of Eq. (27) we do not include sums over vortex-line segments which belong to the thermal loops. In the event that a loop intersects a field induced line, we randomly assign which line segment "belongs" to the field induced line, and which segment "belongs" to the thermally excited loop.

For straight, unentangled vortex lines, we expect that $\langle u^2\rangle$ will saturate to a constant as l_z gets large. For wandering, entangled vortex lines we expect[1] that $\langle u^2\rangle$ will grow with increasing l_z as

$$\langle u^2(l_z)\rangle = u_0^2(T) + D(T) l_z. \tag{28}$$

$D(T)$ measures the diffusion of the line in the transverse direction, as one moves down the $\hat{\mathbf{z}}$ axis, and it can be used to determine the "entanglement correlation length,"[1]

$$\xi_z(T) \equiv \frac{a_v^2}{4D(T)}. \tag{29}$$

ξ_z measures the distance one has to move in the $\hat{\mathbf{z}}$ direction in order to have a transverse fluctuation equal to half the average spacing between the vortex lines. ξ_z is the length scale on which the fluctuating lines can approach each other, leading to a mutual winding and hence entangling.

In Figs. 4(a) and 4(b) we plot $\langle u^2(l_z)\rangle$ versus l_z for several different values of temperature. For $T \geq 2.5J_0 \simeq T_{cz}$ [Fig. 4(a)], the data points for the three largest values of l_z show a clear linear increase with l_z, as expected from Eq. (28) for an entangled phase. For $T < 2.5J_0$ [Fig. 4(b)], there remains a systematic curvature in the data, suggesting a saturation of $\langle u^2\rangle$ at large l_z, as in an unentangled phase; the data here is limited by finite size effects, and runs in a system with larger L_z would be

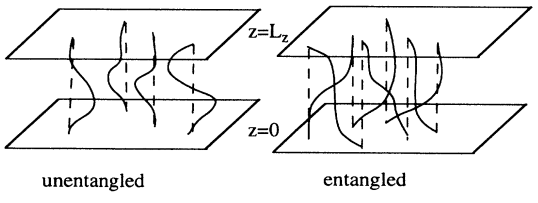

FIG. 3. Schematic showing how vortex lines must connect onto each other, due to the periodic boundary conditions along the $\hat{\mathbf{z}}$ axis. Solid lines represent vortex lines. Dashed lines indicate how the ends of the vortex lines must match up on the $z = 0$ and $z = L_z$ planes.

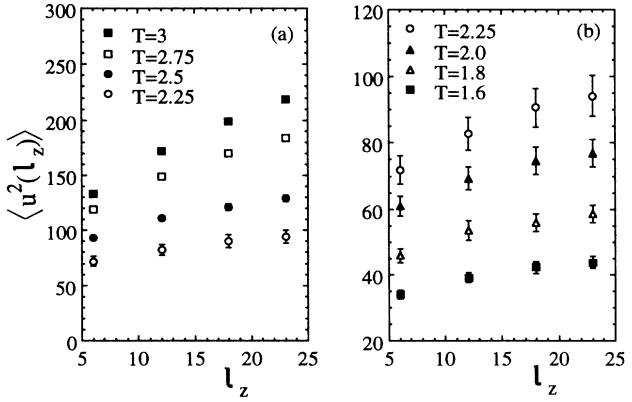

FIG. 4. Transverse fluctuation of vortex lines $\langle u^2\rangle$ as a function of length along the line l_z, for several different temperatures. Linear growth with l_z indicates wandering, entangled lines. Saturation with increasing l_z indicates unentangled lines.

needed in order to clarify the situation. Obtaining $D(T)$ from a fit of Eq. (28) to the three largest values of l_z, for the data of Fig. 4, we compute the resulting ξ_z from Eq. (29) and show the result in Fig. 5.

In a similar manner, we can compute the "cutting correlation length," ξ_c, which we define as the average distance one has to move in the $\hat{\mathbf{z}}$ direction between two successive cuttings of a given vortex line. Within our model, we define a cut as whenever there are two or more vortex lines entering and leaving a given unit cell of the numerical mesh. Such a situation represents an overlapping of the vortex cores, and there is no constraint whatsoever on how the lines will subsequently fluctuate out of this unit cell; lines are free to cut through each other, or even to cut and reconnect different segments of different lines. If N_c is the average number of total cuttings observed in the simulation, then

$$\xi_c(T) \equiv \frac{N_v L_z}{N_c(T)}. \tag{30}$$

We plot $\xi_c(T)$ in Fig. 5.

Comparing the entanglement and cutting correlation lengths, ξ_z and ξ_c, we see that for $T \geq 2.5J_0 \simeq T_{cz}$, $\xi_z \simeq \xi_c$. Thus, entanglement and cutting are occurring on the same length scales for the region above T_{cz}, and here we would expect entanglement to provide little constraint on the motion of vortex lines. Below T_{cz}, we see ξ_c growing faster than ξ_z. However, as discussed above in connection with Fig. 4(b), we believe that our data here is limited by finite size effects, and hence the values shown in Fig. 5 are not a reliable indication of behavior in an infinite sample. It therefore remains unclear whether there exists some narrow range of temperature, at or below T_{cz}, in which entanglement might lead to constraints on vortex-line motion.

Finally, as an additional measure of the fluctuations of the vortex lines, we calculate the average density of vortex lines cutting the planes perpendicular to $\mathbf{B}$,

$$n_v \equiv \frac{1}{N}\sum_i \langle n_z^2(i)\rangle, \tag{31}$$

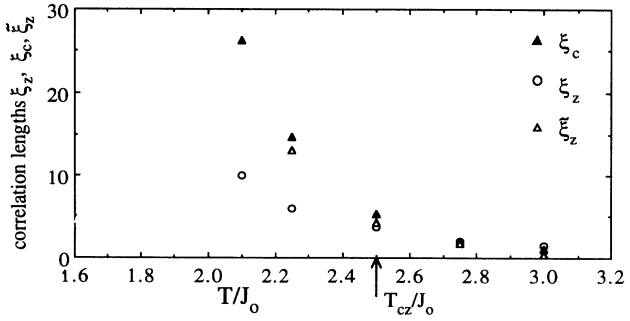

FIG. 5. Correlation lengths along the direction of $\mathbf{B}$. ξ_z is the "entanglement" length, determined by the transverse fluctuations of Fig. 4. ξ_c is the "cutting" length, giving the average distance between two cuttings (intersections) along a single vortex line. $\tilde{\xi}_z$ is the decay correlation length as extracted from the vortex-line structure function, $S(\mathbf{k}_\perp, z)$ (see Sec. III C).

where the sum is over all dual sites i, and $n_z(i)$ is the vorticity passing through the plaquette in the xy plane above site i. In virtually all cases, $n_z = 0, \pm 1$, and so n_v counts the density of lines, irrespective of the sign of the vorticity. If the only vortex lines present in the system are the magnetic field induced lines, and these lines wander through the system in a directed fashion (i.e., all lines pierce each z plane only once; there is no "snaking back") then one has $n_v = f$. If, however, there are additional closed vortex-line loops excited, or lines are not directed, then n_v will be larger than f. In Fig. 6 we plot $n_v(T)$. At low temperatures $T \lesssim 2.0J_0$, we see that $n_v \simeq f$, and hence there are only directed field induced lines. However for $T \gtrsim 2.0J_0$, n_v grows dramatically, becoming $n_v \simeq 2f$ at the transition T_{cz}. Thus, by the time the transition is reached, there are many thermally excited closed vortex loops in the system. This suggests that the transition at T_{cz} is mediated, not by the wandering of the field induced vortex lines, but rather by the proliferation of thermally excited vortex-line loops. The behavior of transverse fluctuations and cuttings, shown in Figs. 4 and 5, may be understood as arising from the growth of loop excitations that intersect and link up neighboring field induced lines, rather than the direct wandering of the field induced lines. In fact, Fig. 6 shows a qualitative resemblance to the density of vortices as one crosses the transition, in the ordinary three-dimensional XY model[29] (corresponding to $\mathbf{B}$=0). Similarly, a plot of the specific heat C, which we compute by numerical differentiation of the average energy and show in Fig. 7, shows the same cusplike feature at T_{cz} as in the 3D XY model.[30] We note that these loop excitations, which we find important for the transition at T_{cz}, are explicitly excluded in the "2D boson" and effective elastic medium approximations for vortex-line fluctuations, as well as in other earlier simulations.[31]

2. *Lower transition* $T_{c\perp}$

The low-temperature phase $T < T_{c\perp}$ is characterized by an ordered vortex-line lattice, with periodicity as given in Fig. 1. The vanishing of $\Upsilon_\perp$ above $T_{c\perp}$, to-

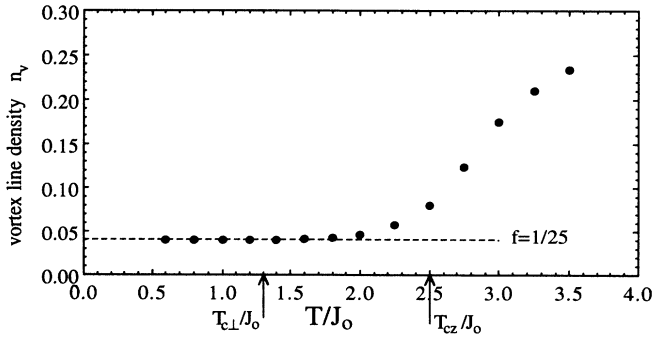

FIG. 6. Average density of vortex lines n_v, piercing planes of constant z. At low T, n_v is the magnetic field induced density of $f = \frac{1}{25}$. n_v increases with T due to the excitation of closed vortex line loops.

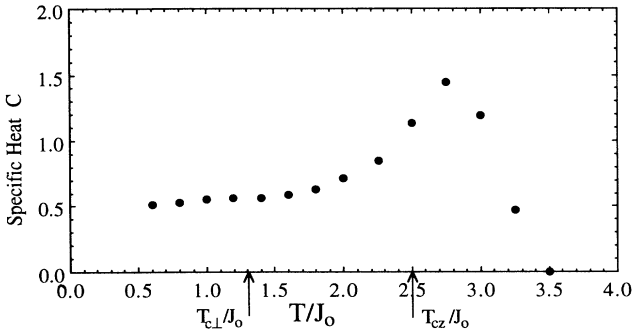

FIG. 7. Specific heat C vs T.

gether with the result that $R \simeq 1$ for $T_{c\perp} < T < T_{cz}$ (see Fig. 2), indicates that that at $T_{c\perp}$ the vortex-line lattice melts into a liquid of unentangled vortex lines. One way to measure this transition is by considering the local orientational order of vortices in the planes perpendicular to $\mathbf{B}$. These vortices are just the intersections of the vortex lines, with a particular plane at constant z. We define the n-fold *local* orientational order, in terms of the quantity

$$\Psi_n = \frac{1}{fN}\sum_{z,i}\frac{1}{M_i}\sum_{j=1}^{M_i} e^{in\phi_{j,j+1}(i)}. \tag{32}$$

In the above, z labels the planes perpendicular to $\mathbf{B}$, i labels the vortices in the plane z, and j labels the M_i nearest-neighbor vortices of i in plane z. $\phi_{j,j+1}(i)$ is the angle between the line from i to j, and the line from i to $j+1$, which is the next neighbor after j which one encounters in rotating around i (see Fig. 8). The nearest neighbors of i are determined by the method of Voronoi polygons.[32] For perfect square orientational order, with all $\phi_{j,j+1}(i) = \pi/2$, such as in the ground state of Fig. 1, we have $\Psi_4 = 1$, while $\Psi_6 = e^{i\pi}$. For perfect hexatic orientational order, with all $\phi_{j,j+1}(i) = \pi/3$, $\Psi_6 = 1$, while $\Psi_4 = e^{i4\pi/3}$. In Figs. 9(a) and 9(b), we plot, respectively, the amplitude and phase of Ψ_4 and Ψ_6. Both amplitudes show a clear kink at $T \simeq 1.3J_0 \simeq T_{c\perp}$. At this temperature, the phases indicate a clear crossover from the fourfold order of the ground state vortex-line lattice, to the local sixfold order of a vortex-line liquid.

For a more global picture of the transition from vortex-line lattice to vortex-line liquid, we have computed the correlation of vortices in the planes perpendicular to $\mathbf{B}$. If we define the vortex structure function[1,9] as

$$S(\mathbf{k}_\perp, k_z) \equiv \frac{1}{N}\langle n_z(\mathbf{k}) n_z(-\mathbf{k})\rangle \tag{33}$$

with $\mathbf{k} = (\mathbf{k}_\perp, k_z)$ and $n_z(\mathbf{k})$ as in Eq. (17), then the correlation between vortices in different planes separated by a height z, is given by the Fourier transform of Eq. (33) with respect to k_z,

$$S(\mathbf{k}_\perp, z) \equiv \frac{1}{L_z}\sum_{k_z} S(\mathbf{k}_\perp, k_z) e^{ik_z z}. \tag{34}$$

The correlation between vortices in the *same* plane is

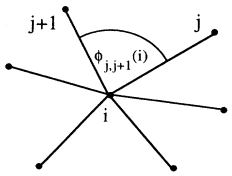

FIG. 8. Schematic showing the measurement of local bond angles $\phi_{j,j+1}(i)$, used for the calculation of local orientational order in Eq. (32).

then just $S(\mathbf{k}_\perp, z = 0)$. In Figs. 10(a)–10(d) we show intensity plots of $S(\mathbf{k}_\perp, z = 0)$ for k_x, k_y in the interval $[-\pi, \pi]$, for several values of temperature, upon heating the system. At $T = 0.6J_0 < T_{c\perp}$ [Fig. 10(a)] we see sharp Bragg peaks, corresponding to the periodic vortex-line lattice of Fig. 1, superimposed on a small continuous background. The width of these Bragg peaks corresponds to the finite resolution of wave vectors allowed by our finite system, $\Delta k_\mu = 2\pi/L_\mu$. At $T = 1.5 \gtrsim T_{c\perp}$ [Fig. 10(b)], we see an approximately rotationally invariant structure, with peaks of finite width. The first peak is at a radius $k_\perp = 2\pi/a_v$, corresponding to the average separation between vortices; the smaller, second peak, is at $k_\perp = 4\pi/a_v$. Such a structure function is characteristic of a liquid. The lack of complete rotational symmetry in the peaks (aside from a slight fourfold distortion to be expected from the underlying cubic mesh) we believe is due to the finite time duration of our simulation; we see no evidence for long range orientational order as might be present in a hexatic line liquid.[33] As T increases [Fig. 10(c)], the second peak disappears into the continuous background. At $T = 2.5J_0 \simeq T_{cz}$ [Fig. 10(d)], both peaks have virtually disappeared, and only a continuous background remains. Thus for $T \gtrsim T_{cz}$, even the short range order, characterized by the average spacing between field induced vortex lines, is lost; this is consistent with the proliferation of many vortex-line loops, as evidenced by Fig. 6.

In the intermediate phase, we find that the system re-

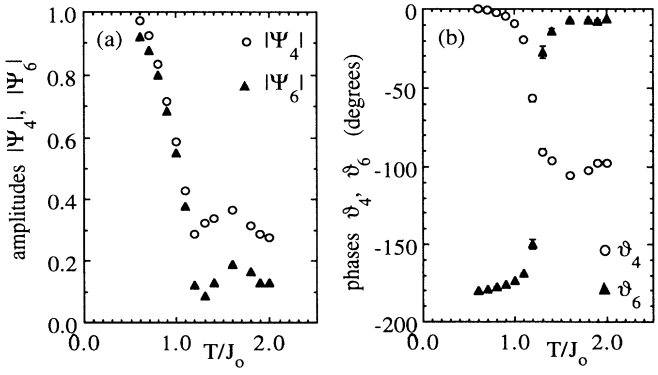

FIG. 9. Fourfold and sixfold local orientational order parameters, $\Psi_4 = |\Psi_4|e^{i\vartheta_4}$ and $\Psi_6 = |\Psi_4|e^{i\vartheta_6}$. The kink in $|\Psi_{4,6}|$ indicates $T_{c\perp} \simeq 1.3J_0$, while the crossover in $\vartheta_{4,6}$ indicates a transition from local fourfold to sixfold order.

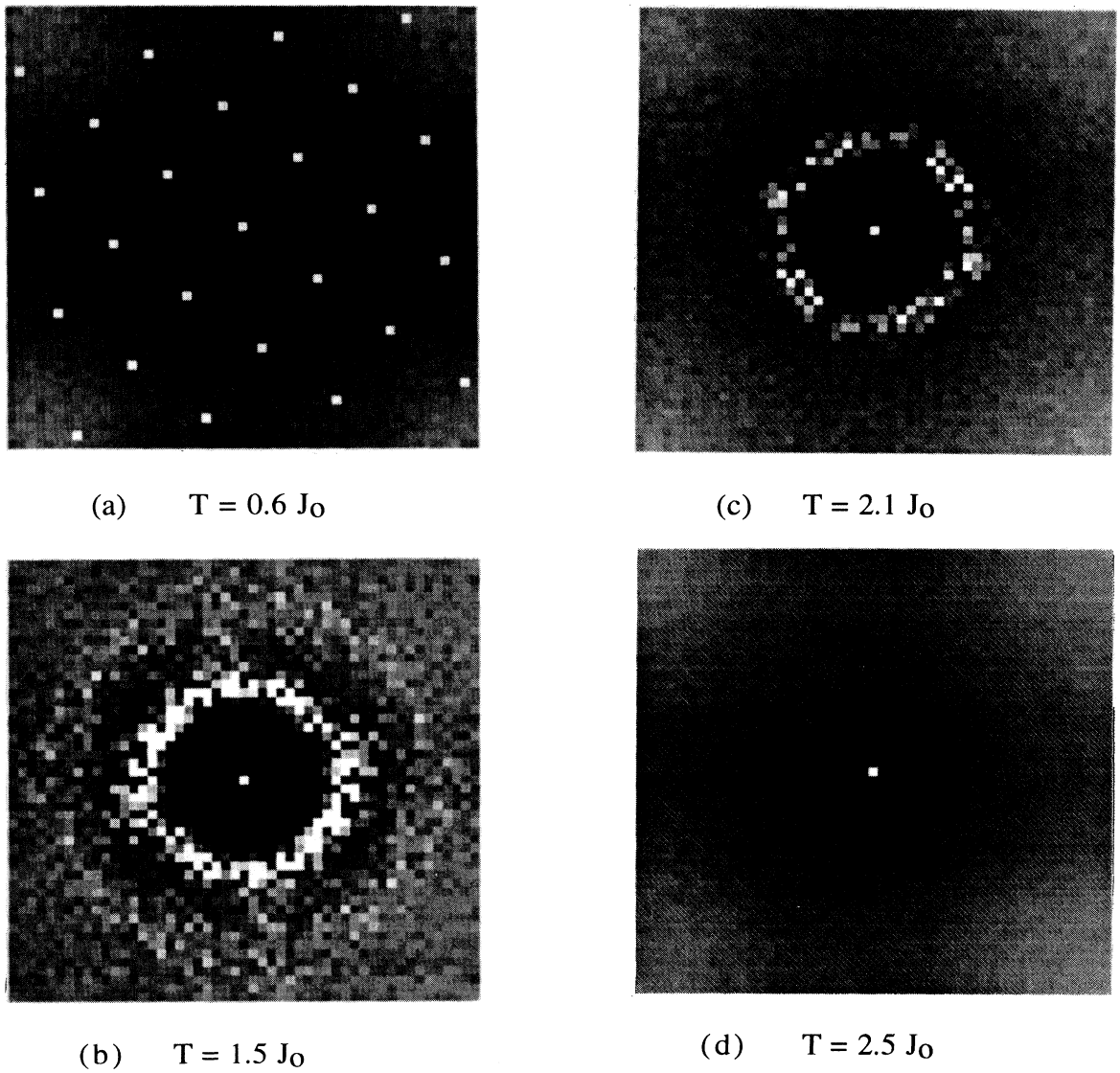

FIG. 10. Intensity plots of vortex structure function $S(\mathbf{k}_\perp, z=0)$, for various temperatures. k_x is the horizontal, and k_y is the vertical direction. Brightness measures the magnitude of S, as in a diffraction pattern. The δ-function peak at $\mathbf{k}_\perp = 0$ is the temperature independent constant $S(0, z=0) = f^2 L_\perp^2$, which sets the relative intensity scale. (a) shows a lattice of Bragg peaks, characteristic of a vortex-line lattice, at $T < T_{c\perp}$. (b) and (c) are characteristic of a vortex-line liquid, for $T_{c\perp} < T < T_{cz}$. (d) is for $T > T_{cz}$, and the dominating continuous background indicates the proliferation of closed vortex-line loop excitations.

laxes *very* slowly to equilibrium. We illustrate this by computing the time dependent correlation

$$g(t) = \frac{1}{N} \sum_i \{\langle n_z(i,t) n_z(i,0)\rangle - \langle n_z(i,t)\rangle \langle n_z(i,0)\rangle\}, \tag{35}$$

where the time t is just the number of Monte Carlo sweeps through the entire cubic mesh. We plot $g(t)$ at $T = 1.9 J_0$ in Fig. 11. After an initial fast decay, we observe a slow algebraic decay, $g(t) \sim t^{-\zeta}$ with $\zeta \simeq 0.23$. We believe that it is this very slow decay which is responsible for the small but finite values of $\Upsilon_\perp$ that are seen for $T > T_{c\perp}$ in Fig. 2, rather than usual finite size effects. When we doubled the number of Monte Carlo steps in our simulation, we observed $\Upsilon_\perp$ in this region to decrease.

Because of this slow equilibration, as the system is cooled back below $T_{c\perp}$, we have been unable to regain the ordered vortex-line lattice of Fig. 1. Instead, we cool into a structure consisting of perfectly straight lines, ordered into local domains of the ground state, with frozen in domain walls. In Fig. 12 we show an intensity plot of $S(\mathbf{k}_\perp, z=0)$ at $T = 0.6 J_0$ for such a cooled configuration. The two rings of peak intensity which exist for $T > T_{c\perp}$ [see Fig. 10(b)], are now narrow and "squared off." This feature of freezing in domain walls, as well as the hysteresis in $\Upsilon_\perp$ seen in Fig. 2, suggest that the tran-

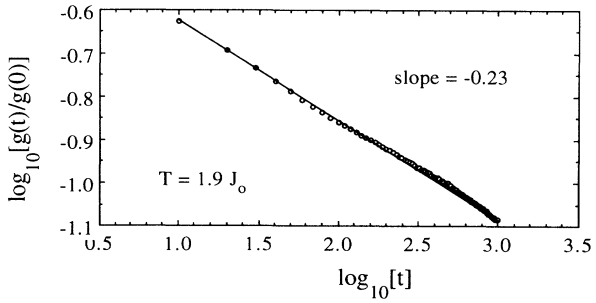

FIG. 11. Time decay of real space vortex correlation function of Eq. (35) for $T = 1.9J_0$, in the intermediate phase. The linear behavior on the log-log plot indicates algebraic decay with the power 0.23. The unit of time is one Monte Carlo sweep through the entire numerical mesh. The solid line is a guide to the eye.

sition at $T_{c\perp}$ may be first order.[34] Another possibility is that $T_{c\perp}$ is not a true thermodynamic transition at all, but only a cross-over depinning temperature where the effective energy barriers to vortex-line motion grow so large that vortex motion is frozen out on the scales of our simulation.

C. Vortex structure function

In Fig. 10, we used the structure function $S(\mathbf{k}_\perp, k_z)$ to qualitatively determine the nature of the vortex-line structure in the different thermodynamic phases. Here we present a more detailed analysis of $S(\mathbf{k}_\perp, k_z)$, from which we can extract information about the effective elastic constants of the model.

Following the works of Marchetti[35] and Nelson and LeDoussal,[9] the natural form for the coarse-grain averaged free energy of our model, valid on *hydrodynamic* length scales $k_\perp^{-1} > a_v$ in the vortex-line liquid phase, is

$$F = \frac{1}{2Nf^2}\sum_{\mathbf{k}}\Big(c_{44}(\mathbf{k}) \sum_{\mu_\perp = x,y} [\delta n_{\mu_\perp}(\mathbf{k})\delta n_{\mu_\perp}(-\mathbf{k})] + c_l(\mathbf{k})\delta n_z(\mathbf{k})\delta n_z(\mathbf{k})\Big), \tag{36}$$

where $\delta n_\mu(\mathbf{k})$ give the deviation from the average uniform density f_μ and are now viewed as independent continuous variables. c_{44} and c_l are the tilt and bulk moduli of the vortex lines on the numerical mesh.

Using the constraint that vortex lines must be continuous, i.e., the discrete divergence of $n_\mu(i)$ vanishes,

$$\sum_\mu [n_\mu(i+\hat{\mu}) - n_\mu(i)] = 0$$

or

$$\sum_\mu n_\mu(\mathbf{k})[e^{ik_\mu} - 1] = 0, \tag{37}$$

one can do the appropriate Gaussian integrals[9] over $\delta n_\mu(\mathbf{k})$ and compute the structure function of Eq. (33):

$$S(\mathbf{k}_\perp, k_z) = \frac{Tf^2K_\perp^2}{c_l(\mathbf{k})K_\perp^2 + c_{44}(\mathbf{k})K_z^2}, \tag{38}$$

where K_μ^2 is related to k_μ as in Eq. (16). The factor $K_\perp^2$ in the numerator of the expression above determines the qualitative form of the continuous background of $S(\mathbf{k}_\perp, z = 0)$ seen in Figs. 10.

From Eq. (36) and the form of the bare vortex-line interaction given in Eqs. (16) and (18), we expect

$$c_l(\mathbf{k}) = 4\pi^2 f^2 J_1 G_k, \quad c_{44}(\mathbf{k}) = c_l(\mathbf{k}) + f\epsilon_1(k_z), \tag{39}$$

where we write J_1 instead of J_0 to allow for possible renormalization of this coupling in the coarse-graining procedure. ϵ_1 is the single vortex-line tension, which depends on k_z, due to the interaction between the different segments of the single line. The difference $c_{44} - c_l$ just gives the additional energy needed to create the elongation of the vortex lines described by the transverse components of the fluctuation.[35] Substituting Eq. (39) into Eq. (38) gives

$$TK_\perp^2/S(\mathbf{k}_\perp, k_z) = 4\pi^2 J_1 + [\epsilon_1(k_z)/f]K_z^2. \tag{40}$$

We now compute $S(\mathbf{k}_\perp, k_z)$ directly within the Monte Carlo simulations. Calculations are done for values of $k_z = 2\pi m_z/L_z$, $m_z = 0, 1, ..., L_z/2$, and for the special values of $\mathbf{k}_\perp = k_\perp\hat{\mathbf{x}}$ and $k_\perp\hat{\mathbf{y}}$, where $k_\perp = 2\pi m_\perp/L_\perp$, $m_\perp = 1, ..., L_\perp/2$. By symmetry, we expect that $S(k_\perp\hat{\mathbf{x}}, k_z) = S(k_\perp\hat{\mathbf{y}}, k_z)$, hence we combine our results by defining $S(k_\perp, k_z)$ as the average of S in these two special directions.

In Figs. 13(a)–13(f), we plot $TK_\perp^2/S$ as a function of $K_\perp^2$ and K_z^2 for temperatures $T = 1.0J_0$ (in the vortex-line lattice phase), $T = 2.25J_0$ (in the intermediate phase), and $T = 2.75J_0$ (in the normal phase). In the line lattice phase [Figs. 13(a) and 13(b)], we see that

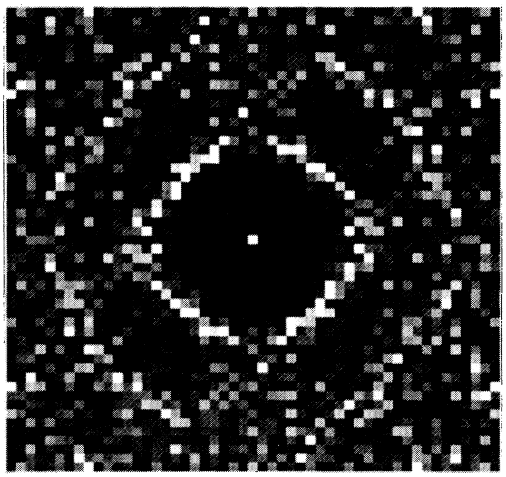

FIG. 12. Intensity plot of vortex structure function $S(\mathbf{k}_\perp, z = 0)$, for $T = 0.6J_0$, upon cooling the system through $T_{c\perp}$.

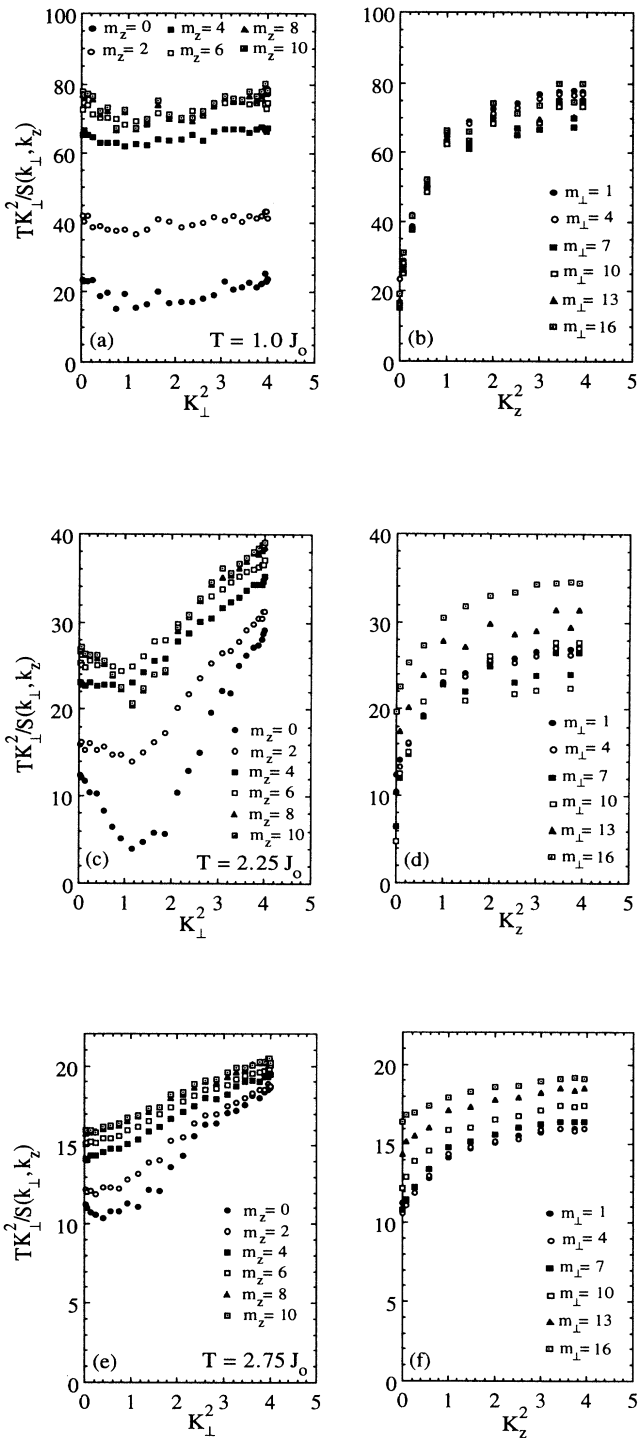

FIG. 13. Structure function data, plotted as $TK_\perp^2/S(k_\perp,k_z)$, vs $K_\perp^2$ and K_z^2, for several different temperatures. K_μ^2 are related to k_μ as in Eq. (16). The different curves vs $K_\perp^2$ are for different values of $k_z = 2\pi m_z/L_z$. The different curves vs K_z^2, are for different values of $k_\perp = 2\pi m_\perp/L_\perp$ ($m_\perp = 10$ corresponds to $k_\perp = 2\pi/a_v$). (a) and (b) are for $T = 1.0J_0$ in the line lattice phase; (c) and (d) are for $T = 2.25J_0$ in the intermediate, unentangled line liquid phase; (e) and (f) are for $T = 2.75J_0$ in the normal, entangled line liquid phase.

$TK_\perp^2/S$ is approximately independent of $k_\perp$, obeying the hydrodynamic form of Eq. (40) at all $\mathbf{k}$. In the intermediate, unentangled line liquid phase [Figs. 13(c) and 13(d), a strong $k_\perp$ dependence appears, with a minimum appearing at $K_\perp^2 \simeq 1.2$, very close to the value of 1.38 which corresponds to $k_\perp = 2\pi/a_v$. In the normal phase [Figs. 13(e) and 13(f)] as T increases, this minimum decreases to smaller $k_\perp$, reflecting the increasing density of vortex lines [see Fig. 6; this also explains why the minimum in Fig. 13(c) is not *exactly* given by $k_\perp = 2\pi/a_v$]. This minimum as a function of $k_\perp$ is a reflection of the peak in $S(\mathbf{k}_\perp, k_z)$ which occurs isotropically in the $\mathbf{k}_\perp$ plane at $|\mathbf{k}_\perp| \simeq 2\pi/a_v$, in the line liquid phase. It may be viewed as an effective softening of the bulk modulus $c_{44}(\mathbf{k})$ at these large values of $k_\perp$. In the line lattice phase, this isotropic peak contracts into discrete Bragg peaks, none of which lie along the $\hat{\mathbf{x}}$ or $\hat{\mathbf{y}}$ directions [see Fig. 10(a)]. Hence the $k_\perp$ dependence of $TK_\perp^2/S$ flattens out.

Although Eqs. (38)–(40) were proposed for the line liquid phase, similar results have been given for the line lattice phase, using an effective elastic approximation.[9] In this case the only change is that one must replace c_l in Eq. (38) with $c_{11} \equiv c_l + c_{66}$, where c_{66} is the shear modulus. This results in the addition of the term $c_{66}K_\perp^2$ to Eq. (40). It is unclear whether or not the differences observed in the $k_\perp$ dependence of Figs. 13(a) and 13(c), may be interpreted in terms of the vanishing of the shear modulus[33] at the melting transition $T_{c\perp}$.

Comparing the curves of $TK_\perp^2/S$ versus K_z^2, for different $k_\perp$, in Figs. 13(d) and 13(f), one sees that the dependence of $TK_\perp^2/S$ on $k_\perp$ and k_z cannot be separated out into the simple form $4\pi^2 J_1(k_\perp) + [\epsilon_1(k_z)/f]K_z^2$ as might be expected from the "2D boson" approximation.[9] As we have noted in earlier work,[13] the more complex dependence we observe may be interpreted as adding a $\mathbf{k}_\perp$ dependence to the line tension ϵ_1. Using Eq. (40) to define the effective line tension as $k_\perp \to 0$,

$$\epsilon_1(k_z) \equiv \frac{f}{K_z^2}\left[\frac{TK_\perp^2}{S(0,k_z)} - \frac{TK_\perp^2}{S(0,0)}\right], \tag{41}$$

we plot in Fig. 14 $\epsilon_1(k_z)$ versus $\ln K_z^2$ for several temperatures T. The plots approach straight lines at large K_z^2. This is in qualitative agreement with the expression for the line tension obtained from an elastic approximation, expanding about the line lattice in a layered superconductor,[5]

$$\epsilon_1(k_z) = \frac{\Phi_0^2}{2(4\pi\lambda)^2}\ln\left[\frac{k_{\perp,\max}^2}{k_{\perp,\min}^2 + K_z^2}\right], \tag{42}$$

where for the line lattice, $k_{\perp,\max} \sim \pi/\xi_0$, and for $\lambda \gg a_v$, $k_{\perp,\min} \sim \pi/a_v$. For our data, we find a reasonable fit with $k_{\perp,\max} \approx \pi$ (in our model $\xi_0 \equiv 1$), but $k_{\perp,\min} \approx 0$.

From the above analysis, we can extract several parameters of interest. Considering the $(k_\perp, k_z) \to 0$ limits, we fit our data to the form of Eq. (40) and extract the values of the hydrodynamic parameters J_1 and $\epsilon_1(0)$, which we plot versus T in Figs. 15(a) and 15(b), respectively. Defining the prefactor of the logarithm in Eq. (42) as

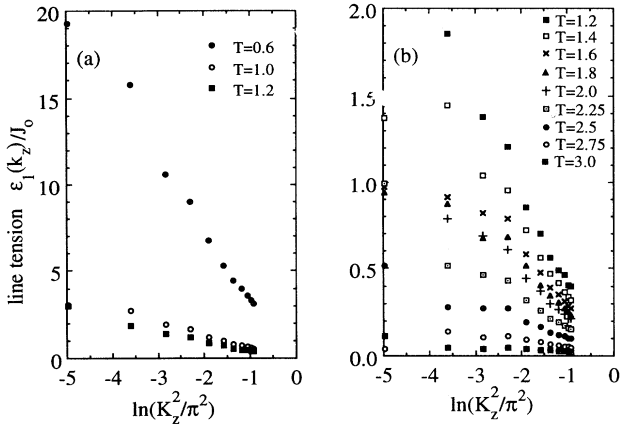

FIG. 14. Line tension $\epsilon_1(k_z)$, from Eq. (41), using data as in Fig. 13. The linear dependence on $\ln K_z^2$, at large K_z^2, agrees qualitatively with the theoretical prediction of Eq. (42). K_z^2 is related to k_z as in Eq. (16).

$(\pi/2)J_2$ [as motivated by Eq. (8)], we can fit the large K_z^2 part of the data in Fig. 14 to $\sim \ln(K_z^2)$ and plot the resulting J_2 in Fig. 15(a). We see that J_1 and J_2 are of comparable magnitude, except at the very lowest temperature $T = 0.6J_0$, and above $T_{cz} \simeq 2.5J_0$, where J_2 decays to zero, while J_1 remains approximately constant.

Finally, we can extract a correlation length along the field direction by computing the Fourier transform of $S(k_\perp, k_z)$ with respect to k_z, as in Eq. (34). Fitting the resulting $S(k_\perp, z)$, at large z, to the form

$$S(k_\perp, z) \simeq S_0(k_\perp)\left[e^{-z/\xi(k_\perp)} + e^{-(L_z-z)/\xi(k_\perp)}\right] \qquad (43)$$

(this form being chosen so as to account for the periodic boundary conditions along $\hat{\mathbf{z}}$), we plot the correlation length $\tilde{\xi}_z \equiv \xi(k_\perp = 2\pi/a_v)$ versus T in Fig. 5. For $T < 2.25J_0$ we found no measurable decay in $S(k_\perp, z)$. For $T \geq 2.25J_0$ we find $\tilde{\xi}_z \approx \xi_c$, the cutting correlation length. This reinforces our earlier observation that cutting and entangling appear to occur on the same length scales. We can use the value of $\tilde{\xi}_z$ just obtained to estimate the hydrodynamic line tension. For finite $\tilde{\xi}_z$, we expect that the effective $k_z \to 0$ line tension can be obtained from Eq. (42) (appropriate for the line lattice where $\tilde{\xi}_z \to \infty$) by imposing a small k_z cutoff at $k_z \simeq \pi/\tilde{\xi}_z$. Hence we estimate

$$\epsilon_1(0) \simeq \epsilon_1(k_z \simeq \pi/\tilde{\xi}_z) \simeq \pi J_2 \ln \tilde{\xi}_z. \qquad (44)$$

We plot the result in Fig. 15(b), where we have set $\tilde{\xi}_z \equiv L_z$ for all $T < T_{cz}$. Although we observe quite reasonable agreement with the hydrodynamic result obtained from a direct fit to Eq. (40), we note that the dominant temperature dependence comes from the behavior of J_2. We do not have large enough of a range of $\tilde{\xi}_z$ to provide a sensitive test of the $\ln \tilde{\xi}_z$ dependence.

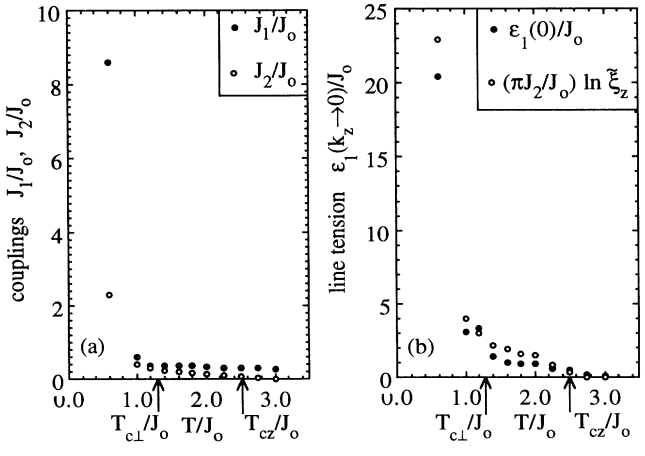

FIG. 15. (a) Coupling J_1, and (b) line tension $\epsilon_1(k_z \to 0)$, obtained from a fit of $TK_\perp^2/S$ to the hydrodynamic limit, Eq. (40). (a) Coupling J_2, obtained from a high K_z^2 fit of the line tension data of Fig. 14, to the form Eq. (42). (b) Hydrodynamic line tension $\pi J_2 \ln \tilde{\xi}_z$ obtained from Eq. (44), using the structure function correlation length $\tilde{\xi}_z$ of Fig. 5.

IV. CONCLUSIONS AND DISCUSSION

To conclude, we have studied a model of fluctuating vortex lines, and find three distinct thermodynamic phases. Upon heating, the system has sharp transitions from a vortex-line lattice, to an unentangled vortex-line liquid, to an entangled vortex-line liquid with many closed vortex-line loops and much vortex-line cutting. The lower transition is associated with the loss of phase coherence in the superconducting order parameter, in directions perpendicular to the applied magnetic field. The upper transition is associated with the loss of phase coherence in the parallel direction. This behavior is consistent with that argued by Feigel'man and co-workers.[26] Similar behavior has been argued by Glazman and Koshelev,[5] for low magnetic fields $B < B_{cr}$.[36] Nelson[2] originally suggested an unentangled line liquid phase as a finite size effect, when $\xi_z \approx L_z$. We cannot rule out the possibility that the difference we observe between $T_{c\perp}$ and T_{cz} is such a finite size effect. However, if this is so, our observation that $T_{cz} \simeq 2T_{c\perp}$ would indicate a rather large critical region about the single transition of the infinite system. Similarly, more detailed finite size studies would be needed for one to clarify the *nature* of the phase transitions in our model. In our earlier work,[12,13] at the higher density $f = \frac{1}{5}$, we found evidence for only a single transition. It may be that there is indeed only a single transition at higher densities, or it may be that the width of the intermediate region becomes too narrow to distinguish. It is interesting to note that in a related model, the 3D XY model of stacked triangular planes with antiferromagnetic coupling within the triangular planes and ferromagnetic coupling between the planes, which has the same symmetry[37] as our model with $f = \frac{1}{2}$, there is only a single transition, however, it is a tetracritical point.[38]

Our model has involved two key approximations in its mapping to a realistic superconductor. One is the dis-

cretization of space into a cubic mesh, on the length scale of the bare coherence length ξ_0. The discretization along the $\hat{\mathbf{z}}$ axis may be viewed as representing the layered structure of the high-T_c materials, as in a Lawrence-Doniach model.[39] The discretization in the xy plane, however, represents an artificial periodic pinning potential for vortex-line fluctuations. Our hope was that this pinning potential primarily acts to remove the mode associated with a uniform translation of the entire vortex-line lattice. However the "forces" associated with this pinning potential are strong enough to tilt the balance in favor of a square line lattice in the ground state, as opposed to the triangular lattice expected in a continuum. One may worry that these forces also significantly suppress vortex-line fluctuations, leading to a stabilization of the line lattice, as well as phase coherence of the superconducting order parameter, at low temperatures. However, in Figs. 15 we see a sharp drop in J_1 and $\epsilon_1(0)$ at $\tilde{T} < 1.0J_0$, noticeably below the lower transition $T_{c\perp} \simeq 1.3J_0$. If we interpret $\tilde{T}$ as the energy scale associated with the energy barriers of the periodic pinning potential, then one expects that the transition at $T_{c\perp}$ is a true melting transition of the line lattice, rather than just a depinning of the lines.

The second approximation has been the assumption of a uniform magnetic induction $\mathbf{B}$ inside the superconductor, i.e., the $\lambda \to \infty$ limit. We first discuss the effects of this approximation on vortex-line fluctuations. As mentioned in Sec. II, setting $\lambda \to \infty$ suppresses long wavelength (small $k < \lambda^{-1}$) density fluctuations, while being a good approximation for high $k \gtrsim \lambda^{-1}$ fluctuations. It is generally believed,[4,5] however, that it is high $k_\perp \simeq 2\pi/a_v$ shear fluctuations, which do not alter the long wavelength density, that are responsible for melting of the vortex-line lattice. Ikeda *et al.*[40] specifically note that the melting transition, as determined from a Lindemann criterion, is largely unaffected when comparing the finite λ to the $\lambda \to \infty$ cases, providing $\lambda \gg a_v$. Hence we expect behavior in the line lattice phase, and the melting at $T_{c\perp}$, to be largely independent of this uniform $\mathbf{B}$ approximation. Similarly, in the normal, entangled line liquid phase, $T > T_{cz}$, one expects this approximation to be good for describing *local* properties [such as entangling, cutting, and $S(\mathbf{k})$ for $k > \lambda^{-1}$] provided $\lambda \gg \tilde{\xi}_z$, the correlation length along the $\hat{\mathbf{z}}$ axis. In this case, fluctuations impose a shorter cutoff on effective interactions than does magnetic screening. It is less clear how valid the approximation is in the intermediate phase, where $\tilde{\xi}_z \to \infty$, and there is no other natural length scale along the $\hat{\mathbf{z}}$ direction with which to compare λ. However we note that Feigel'man[26] predicts a similar unentangled phase, working within the "2D boson" approximation, in which the interaction between vortex lines along the $\hat{\mathbf{z}}$ direction is short ranged. Further work will be necessary to determine whether the unentangled line liquid phase observed here, is stable against fluctuations of $\mathbf{B}$.

The effect of the $\lambda \to \infty$ approximation on fluctuations of the phase of the superconducting order parameter, and the existence of true long range order in the gauge invariant order parameter correlation function, has been a subject of much discussion.[5,40–42] Moore[41] and Ikeda *et al.*[40] have shown that in three dimensions, the gauge invariant order parameter correlations decay algebraically, in the line lattice phase, for the $\lambda \to \infty$ case. However for the finite λ case, they decay exponentially. Such algebraic decay is consistent with a finite helicity modulus[43] Υ, as we observe in our model. Exponential decay, for finite λ, would imply $\Upsilon \to 0$. However as shown in Refs. 40 and 41, the length scale for such exponential decay is given by $(\pi J_0/T)\lambda\kappa$, and is hence comparable to the size of macroscopic samples, for the large κ high-T_c materials. Thus the $\lambda \to \infty$ limit should be appropriate in such situations.[44]

Although we have not attempted any direct mapping between our model and a specific high-T_c material (we took isotropic couplings, and ignored all T dependences of our bare parameter J_0), it is tempting to try to discuss resistivity measurements in very pure YBCO single crystals,[7,45] in terms of the behavior we observe in our model. Above the upper transition T_{cz}, where there are many vortex-line loops, much wandering and entangling of the field induced vortex lines, and easy cutting of vortex lines, we might expect substantial flux flow resistance due to the flow of effectively *independent* vortex-line segments. This region possibly describes much of the broadening of the resistive transition, in comparison to the $B = 0$ case, and could be explained with traditional flux flow models.[46] Resistivity, ρ_z, for current $I \parallel B$, should be comparable to $\rho_\perp$ for $I \perp B$ (apart from effects due to explicit anisotropy of couplings), as there are almost as many vortex-line segments oriented perpendicular to B as parallel to B (from closed loops, and transverse segments of wandering lines). As T is cooled towards T_{cz} we would expect ρ_z to decrease substantially compared to $\rho_\perp$, as the vortex lines disentangle, and straighten parallel to B, and there are fewer loop excitations. Such behavior is consistent with that seen in experiments[45] where $\mathbf{B}$ is applied in the ab (CuO) planes, and hence there is no explicit anisotropy effects for ρ_z versus $\rho_\perp$. Below T_{cz}, the linear resistivity ρ_z should vanish, however the linear part of $\rho_\perp$ would remain finite. The transition at T_{cz} might offer an explanation for the "kink" observed in $\rho_\perp$ in the tail of the resistance curve, for very pure samples with $\mathbf{B}$ along the c axis.[7] Finally, $\rho_\perp$ would vanish below $T_{c\perp}$.

ACKNOWLEDGMENT

This work was supported by Grant No. DE-FG02-89ER14017 from the U.S. Department of Energy.

[1] D. R. Nelson and H. S. Seung, Phys. Rev. B **39**, 9153 (1989).
[2] D. R. Nelson, Phys. Rev. Lett. **60**, 1973 (1988); J. Stat. Phys. **57**, 511 (1989).
[3] D. S. Fisher, M. P. A. Fisher, and D. A. Huse, Phys. Rev. B **43**, 130 (1991).
[4] A. Houghton, R. A. Pelcovits, and A. Sudbø, Phys. Rev. B **40**, 6763 (1989); E. H. Brandt, Phys. Rev. Lett. **63**, 1106 (1989); M.A. Moore, Phys. Rev. B **39**, 136 (1989).

[5]L. I. Glazman and A. E. Koshelev, Phys. Rev. B **43**, 2835 (1991).
[6]P. L. Gammel, L. F. Schneemeyer, J. V. Wasczczak, and D. J. Bishop, Phys. Rev. Lett. **61**, 1666 (1988); D. E. Farrell, J. P. Price, and D. M. Ginsberg, *ibid.* **67**, 1165 (1991); R. G. Beck, D. E. Farrell, J. P. Rice, D. M. Ginsberg, and V. G. Kogan, *ibid.* **68**, 1594 (1992).
[7]T. K. Worthington, F. H. Holtzberg, and C. A. Field, Cryogenics **30**, 417 (1990); U. Welp, W. K. Kwok, G. W. Crabtree, K. G. Vandervoort, and J. Z. Liu, Phys. Rev. Lett. **62**, 1908 (1989).
[8]E. H. Brandt, J. Low Temp. Phys. **26**, 735 (1977); A. Sudbø and E. H. Brandt, Phys. Rev. Lett. **66**, 1781 (1991).
[9]D. R. Nelson and P. LeDoussal, Phys. Rev. B **42**, 10113 (1990).
[10]P. Minnhagen and P. Olsson, Phys. Rev. Lett. **67**, 1039 (1991).
[11]G. Carneiro, Phys. Rev. B **45**, 2391 (1992); **45**, 2403 (1992).
[12]Y.-H. Li and S. Teitel, Phys. Rev. Lett. **66**, 3301 (1991).
[13]Y.-H. Li and S. Teitel, Phys. Rev. B **45**, 5718 (1992).
[14]M. Tinkham, *Introduction to Superconductivity* (Krieger, Malabar, FL, 1980).
[15]For a discussion of a similar lattice superconductor with $\mathbf{B} = \mathbf{0}$, see C. Dasgupta and B. I. Halperin, Phys. Rev. Lett. **47**, 1556 (1981).
[16]A mapping that allows one to obtain results for systems with anisotropic couplings, in terms of an equivalent isotropic system, is given in G. Blatter, V. B. Geshkenbein, and A. I. Larkin, Phys. Rev. Lett. **68**, 875 (1992).
[17]S. Teitel and C. Jayaprakash, Phys. Rev. Lett. **51**, 1999 (1983).
[18]For a review of recent work, see articles in *Proceedings of NATO Advanced Research Workshop on Coherence in Superconducting Networks*, edited by J. E. Mooij and G. B. Schön [Physica B **152**, 1 (1988)].
[19]W. Y. Shih, C. Ebner, and D. Stroud, Phys. Rev. B **30**, 134 (1984); D. A. Huse and H. S. Seung, *ibid.* **42**, 1059 (1990).
[20]J. Villain, J. Phys. (Paris) **36**, 581 (1975).
[21]E. Fradkin, B. Huberman, and S. Shenker, Phys. Rev. B **18**, 4789 (1978).
[22]E. H. Brandt, in *Proceedings of the International Conference on Low Temperature Physics, LT-19*, edited by D. S. Betts [Physica B **165&166**, 1129 (1990)]; Int. J. Mod. Phys. B **5**, 751 (1991).
[23]R. Cavalcanti, B. Carneiro, and A. Gartner, Europhys. Lett. **17**, 449 (1992).
[24]M. E. Fisher, M. N. Barber, and D. Jasnow, Phys. Rev. A **8**, 1111 (1973).
[25]S. Teitel and C. Jayaprakash, Phys. Rev. B **27**, 598 (1983).
[26]M. V. Feigel'man, Physica A **168**, 319 (1990); M. V. Feigel'man, V. B. Geshkenbein, and V. M. Vinokur, Pis'ma Zh. Eksp. Teor. Fiz. **52**, 1141 (1990) [JETP Lett. **52**, 546 (1990)].
[27]M. C. Marchetti and D. R. Nelson, Phys. Rev. B **42**, 9938 (1990); Physica C **174**, 40 (1991).
[28]S. P. Obukhov and M. Rubinstein, Phys. Rev. Lett. **65**, 1279 (1990); **66**, 2279 (1991).
[29]G. Kohring, R. Schrock, and P. Wills, Phys. Rev. Lett. **57**, 1358 (1986).
[30]Y.-H. Li and S. Teitel, Phys. Rev. B **40**, 9122 (1989).
[31]S. Ryu, S. Doniach, G. Deutscher, and A. Kapitulnik, Phys. Rev. Lett. **68**, 710 (1992); H.-r. Ma and S. T. Chui, *ibid.* **68**, 2528 (1992); L. Xing and Z. Tešanović, *ibid.* **65**, 794 (1990)
[32]H. S. M. Coxeter, *Introduction to Geometry* (Wiley, New York, 1961), p. 53. In order to ensure that we do not triangulate square unit cells, we use the following prescription: Each pair of points i and j are joined with a tentative bond. For every other point k within a fixed range of i and j, we measure the angle ikj. If this angle is larger or equal to 90°, we remove the bond ij.
[33]M. C. Marchetti and D. R. Nelson, Phys. Rev. B **41**, 1910 (1990).
[34]For a finite-size analysis that indicates this transition is first order in a closely related model, see R. E. Hetzel, A. Sudbø, and D. A. Huse, Phys. Rev. Lett. **69**, 518 (1992).
[35]M. C. Marchetti, Phys. Rev. B **43**, 8012 (1991).
[36]However, according to their estimate of B_{cr} [see Eq. (5) of Ref. 5], we believe our model lies in the region $B > B_{cr}$.
[37]D. H. Lee, J. D. Joannopoulos, J. W. Negele, and D. P. Landau, Phys. Rev. B **33**, 450 (1986).
[38]H. Kawamura, A. Caillé, and M. L. Plumer, Phys. Rev. B **41**, 4416 (1990).
[39]W. E. Lawrence and S. Doniach, in *Proceedings of the International Conference on Low Temperature Physics, LT-12, Kyoto, 1970*, edited by E. Kanda (Keigaku, Tokyo, 1971), p. 361.
[40]R. Ikeda, T. Ohmi, and T. Tsuneto, J. Phys. Soc. Jpn. **61**, 254 (1992).
[41]M. A. Moore, Phys. Rev. B **45**, 7336 (1992).
[42]A. Houghton, R. A. Pelcovits, and A. Sudbø, Phys. Rev. B **42**, 906 (1990).
[43]Such is the case, for example, in the Kosterlitz-Thouless transition of the ordinary 2D XY model; see T. Ohta and D. Jasnow, Phys. Rev. B **20**, 139 (1979).
[44]In Ref. 40 it is argued that for both the finite λ and the $\lambda \to \infty$ cases, the order parameter correlations, both perpendicular and parallel to $\mathbf{B}$, become short ranged once the shear modulus $c_{66} \to 0$. This would appear to contradict the observation in our model that $\Upsilon_z > 0$ in the intermediate phase, where presumably $c_{66} = 0$. Our results also contradict the prediction of Ref. 5, that phase coherence parallel to $\mathbf{B}$ is lost at a temperature much below the melting transition of the vortex-line lattice.
[45]W. K. Kwok, U. Welp, G. W. Crabtree, K. G. Vandervoort, R. Hultscher, and J. Z. Liu, Phys. Rev. Lett. **64**, 966 (1990).
[46]M. Tinkham, Phys. Rev. Lett. **61**, 1658 (1988).

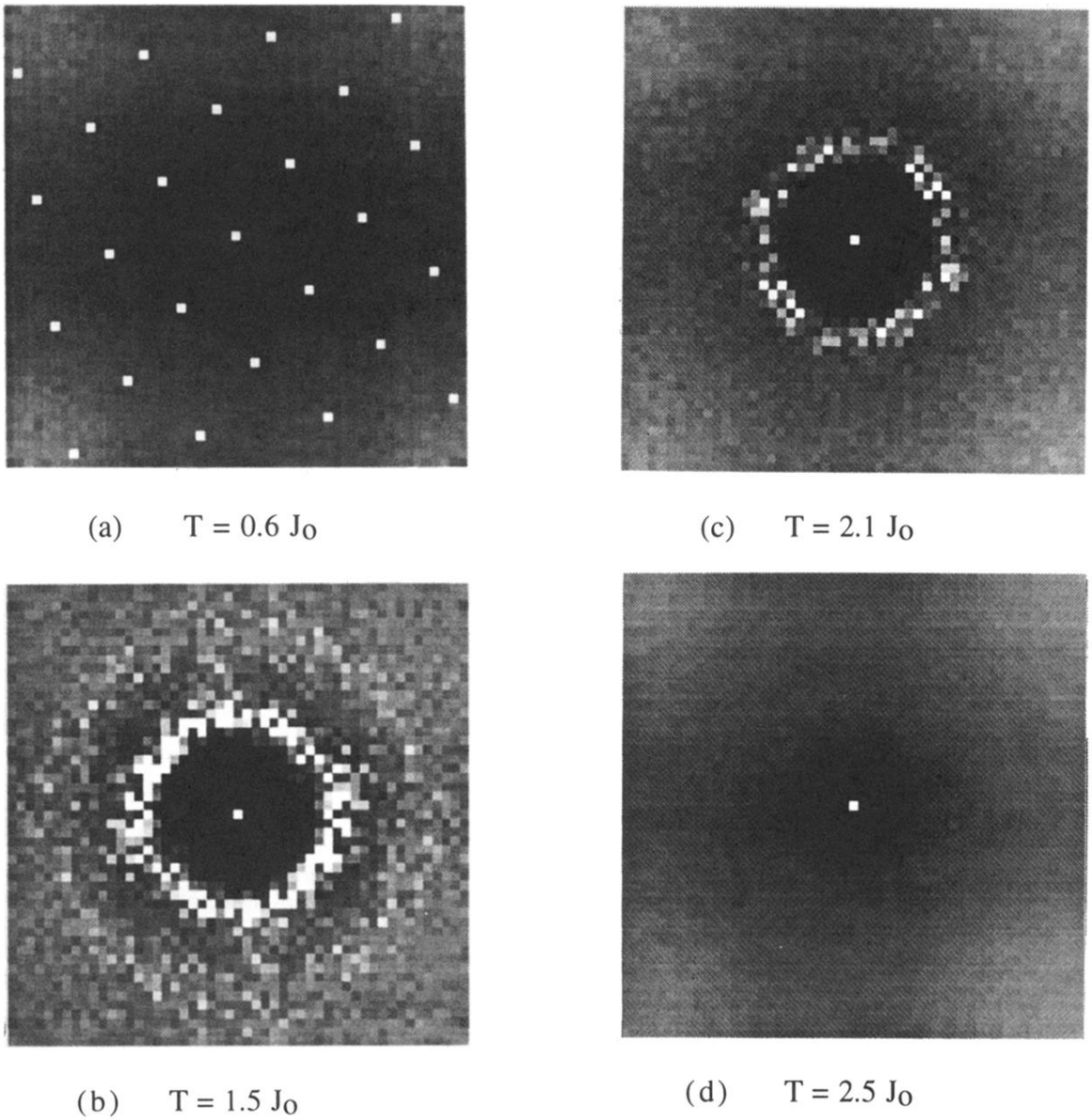

FIG. 10. Intensity plots of vortex structure function $S(\mathbf{k}_\perp, z = 0)$, for various temperatures. k_x is the horizontal, and k_y is the vertical direction. Brightness measures the magnitude of S, as in a diffraction pattern. The δ-function peak at $\mathbf{k}_\perp = 0$ is the temperature independent constant $S(0, z = 0) = f^2 L_\perp^2$, which sets the relative intensity scale. (a) shows a lattice of Bragg peaks, characteristic of a vortex-line lattice, at $T < T_{c\perp}$. (b) and (c) are characteristic of a vortex-line liquid, for $T_{c\perp} < T < T_{cz}$. (d) is for $T > T_{cz}$, and the dominating continuous background indicates the proliferation of closed vortex-line loop excitations.